A membrane-less Glucose/O2 non-enzymatic fuel cell based on bimetallic Pd–Au nanostructure anode and air-breathing cathode: Towards micro-power applications at neutral pH

Abdelghani Ghanam, Naoufel Haddour, Hasna Mohammadi, Aziz Amine, Andrei Sabac, François Buret

A Membrane-less Glucose/O_2 Non-enzymatic Fuel Cell Based on Bimetallic Pd-Au Nanostructure Anode and Air-breathing Cathode: Towards Micro-power Applications at Neutral pH

Abdelghani Ghanam[a, b], Naoufel Haddour[b*], Hasna Mohammadi[a], Aziz Amine[a*], Andrei Sabac[b], François Buret [b]

[a] Chemical Analysis and Biosensors Group, Laboratory of Process Engineering and Environment, Faculty of Sciences and Techniques, Hassan II University of Casablanca, B.P 146, Mohammedia, Morocco.

[b] Univ Lyon, Ecole Centrale de Lyon, INSA Lyon, Université Claude Bernard Lyon 1, CNRS, Ampère, UMR5005, 69130 Ecully, France.

*Corresponding authors: a.amine@univh2m.ac.ma (A. Amine); naoufel.haddour@ec-lyon.fr (N. Haddour)

ORCID IDs:
AG: 0000-0003-1634-7351
NH: 0000-0002-2430-5568
HM: 0000-0003-1506-8481
AA: 0000-0001-7909-2224
AS: 0000-0001-9305-1701
FB: 0000-0002-6924-5909

Abstract

Herein, the authors propose a miniaturized glucose/O_2 n-EFC based on a new direct electron transfer. The anode is a screen-printed carbon electrode (SPCE) modified with functionalized carbon nanotubes (f-CNTs) and cauliflower-like PdAu nanostructures (PdAuNS). The PdAuNS/f-CNT biomimetic nanocatalyst was prepared using a cost-effective and straightforward method, which consisted of drop-casting well-dispersed f-CNTs over the SPCE surface before PdAuNS electrodeposition. This enzyme-free interface was used for glucose electrooxidation at neutral medium (pH 7.4). The electrochemical behaviour of the PdAuNS/f-CNT/SPCE was investigated using cyclic voltammetry, linear sweep voltammetry, and amperometry. Several parameters were optimized and discussed, including the metal precursor concentration ($HAuCl_4$, $PdCl_2$) and the electrodeposition conditions. The cathode for oxygen electroreduction is an air-cathode which is composed of Pt-coated carbon cloth. The electrochemical performances of the anode and the cathode were evaluated separately for glucose oxidation and oxygen reduction, respectively. Both electrodes were then assembled in a membrane-less single chamber n-EFC with an innovative architecture. Electrical characterization of the n-EFC supplied with a neutral buffered solution containing 20 mM glucose showed a maximal power output of 129 ± 11 $\mu W.cm^{-2}$, a current density of 600 ± 39 $\mu A.cm^{-2}$ with a cell voltage of 0.35 V, and an open circuit potential of 0.56 V. The proposed electrocatalyst possesses several advantages such as fast response, low cost, reusability, poison-free characteristics, and good stability. Hence, glucose/O_2 n-EFC could be of great interest in direct glucose fuel cell applications (e.g., powering mountable/implantable biomedical micro-devices running at low electrical power supply) or in self-powered biosensing.

Keywords: Non-enzymatic fuel cell, membrane-less fuel cell, Pd-Au electrocatalyst, glucose, air-breathing cathode

RESEARCH HIGHLIGHTS

- Porous cauliflowers-like PdAu nanostructures (PdAuNS), as enzyme-free electrocatalysts, were prepared by a facile co-electrodeposition method.
- A promising membrane-less non-enzymatic fuel cell (n-EFC) architecture to output a stable power density in neutral pH directly proportional to the glucose concentration.
- A first air-breathing cathode n-EFC was developed.
- With air cathodes, there is no need for air bubbling or air-saturating conditions to operate the glucose-O_2 n-EFC.
- A maximum power density of 129 ± 11 $\mu W.cm^{-2}$ at +0.35 V and at 20 mM glucose was reached.

1. Introduction

Glucose is recognized as the most essential energy source for many living organisms (Chu et al., 2020; Cosnier et al., 2014; Mergenthaler et al., 2013). Glucose Electrooxidation Reaction (GOR) has been of great interest, not only in the development of new electrochemical glucose monitoring systems but also for implantable glucose fuel cells (GFCs) (Chansaenpak et al., 2021; Pakapongpan et al., 2017). Because of its characteristics, such as natural abundance, sustainability, non-toxicity, no storage complications as well as ease of production, glucose is a desirable fuel for GFC technologies (Antolini, 2021; Elouarzaki et al., 2016, 2012; Kim and Yoon, 2021). GFC is an electrochemical system that directly converts the chemical energy of glucose into electrical energy via an electrochemical process using enzymes or metal-based catalysts (Y. Chen et al., 2019; Cosnier et al., 2016). The common reactions catalyzed in a GFC are the oxidation of glucose to gluconolactone at the anode and the reduction of oxygen to water at the cathode. GFC is a sustainable and eco-friendly power generation technology that has attracted much research attention over the last few years (Brouzgou and Tsiakaras, 2015; Kim and Yoon, 2021). This new electrochemical technology could be used as a power source to supply mountable or implantable biomedical devices running at low electrical power for electrical stimulation (e.g., pacemakers, artificial hearts, insulin pumps, etc.) and implantable (bio)sensors (Cosnier et al., 2014; Santiago et al., 2016). Additionally, GFCs can act as self-powered wearable electrochemical sensors for real-time monitoring and Point-of-Care (POC) diagnosis of diabetes. (Cosnier et al., 2014). They require no battery or external power supply; they collect chemical energy from the medium and perform self-supply of electricity for detection through the electrochemical process (i.e., GFC output power) (Y. Chen et al., 2019; Dutta et al., 2022). Glucose has a theoretical energy density (4430 $W.h.kg^{-1}$) close to that of methanol (6100 $W.h.kg^{-1}$) (Santiago et al., 2016), making it a very interesting fuel. Furthermore, it is an endogenous substance in body fluids, raising the possibility of its use with dissolved oxygen in body fluids in an implantable/mountable glucose-O_2 fuel cell. Therefore, there has been an increasing demand for the development of inexpensive electrocatalysts that are characterized by high sensitivity, good stability, and low overpotential for glucose oxidation (Adeel et al., 2020). GOR was usually catalyzed either by enzymes or nanomaterial-based abiotic electrocatalysts.

Accordingly, GFCs can be divided into enzymatic and non-enzymatic electrochemical systems. The first glucose biofuel cell was demonstrated by (Yahiro et al., 1964) and

consisted of an enzyme-modified bioanode and a Pt cathode to indirectly convert glucose chemical energy into electricity. Generally, glucose oxidase (GOx) and glucose dehydrogenase (GDH) biocatalysts are the most commonly used enzymes in enzymatic GFCs (Cadet et al., 2016; Cosnier et al., 2016). Natural enzymes have shown their potential in the enzymatic biofuel cell (EBC) research field in many reported studies (Dutta et al., 2022; Zhang et al., 2021). They are suitable and safe for body-implantable devices in many living species in addition to demonstrating excellent selectivity and sensitivity towards their substrates. However, these bioelectrochemical systems are still facing some challenges, limiting their long-term *in vivo* application and commercialization, such as manufacturing cost, low output power, and poor stability of enzymes (Adeel et al., 2020; Ghica et al., 2013; Wilson and Turner, 1992). In addition, their application in enzyme-based biosensors for indirect glucose monitoring requires cumbersome immobilization procedures, stringent storage conditions, and a relatively high positive potential to oxidize hydrogen peroxide (H_2O_2) produced by the enzymatic reaction (Adeel et al., 2020; Huang et al., 2018). Therefore, there is a real need to develop either nanomaterial for an enzyme-mimicking activity or artificial/simulated enzymes to replace natural enzymes. To overcome enzyme-related drawbacks, efforts are being made to develop glucose-O_2 non-enzymatic fuel cells (n-EFC) like abiotic systems based on noble metal nanostructures (Au, Pt, etc.). Indeed, Pt is the first material discovered and widely studied for glucose electrooxidation (Jiang et al., 2015). However, Pt-based catalysts are unsuitable to be embedded into wearable glucose-O_2 n-EFC devices. This is due to their high chemosorbability for various compounds present in physiological solutions that block catalytic sites (Vassilyev et al., 1985). In contrast, Au has shown a remarkable electrocatalytic activity for glucose electrooxidation and poison tolerance for glucose oxidation products in alkaline and neutral environments (Yan et al., 2014). Yet, the electrooxidation of glucose on the Au catalyst occurs at an excessively high potential contributing to substantial energy loss (Aoun et al., 2003). Several studies have described the electrocatalytic activity of carbon nanotubes (CNTs) modified with various Pd-based nanostructures. The use of CNTs as carbon-based supporting materials has been an important strategy in the construction of non-enzymatic electrocatalysts electrocatalysts. They increase electroactive surface area for immobilization of metallic nanomaterials and improve their chemical stability and electrical conductivity (Qu and Dai, 2005; Valentini et al., 2003). Additionally, Pd possesses outstanding characteristics, including biocompatibility and high electrocatalytic activity towards glucose electrooxidation at a lower overpotential (Samoson et al., 2019). Pd/Au alloy catalysts are mostly adopted for GOR to achieve a synergistic effect

by harnessing the unique properties of each metal. This binary system based on Pd and Au metals often exhibits better electrocatalytic activity than the individual metals. For instance, (Jiang et al., 2015) reported excellent GOR performance of Pd/Au chemically synthesized. (Yan et al., 2014) described the ability of chemically prepared Pd/Au alloy catalysts to electrocatalyse glucose oxidation, showing promising performance for the development of glucose sensors and direct glucose fuel cells. In comparison with the chemical methods used in these studies for catalyst preparation, electrochemical deposition is a flexible technique allowing rapid coating of electrodes with thin films of catalysts of different sizes (micro- and nano-structures) and forms (wires, rods, tubes, ribbons…) (Shu et al., 2014; Sun and Chang, 2017; Tian et al., 2009; Wei et al., 2012). The shape and size of metal-based catalysts have a significant effect on electrocatalytic activity (Ye et al., 2015). To the best of our knowledge, electrocatalytic performance of the electrodeposited Pd/Au alloy catalysts for GOR has not been investigated to date, although this preparation method provides the opportunity for controlling the shape and size of the deposited catalysts through electrolysis parameters (applied potential, concentration of the metallic precursors, temperature, pH, time duration of the electrolysis…) (Low et al., 2006). Furthermore, the electrocatalytic activity of these metal-based catalysts requires alkaline conditions limiting their incorporation into a physiological environment. Most glucose-O_2 n-EFC are still designed to work in highly alkaline media of 0.5 M KOH (Chu et al., 2013). One example comes from a recent study that reported a dual-compartment non-enzymatic glucose fuel cell using a nano/micro hybrid-structured Au anode operating in an alkaline anolyte of 1.0 M NaOH, pH 14.0 (Chu et al., 2020).

Moreover, most glucose-O_2 n-EFC devices were operated in an O_2-saturated environment (Chu et al., 2021; Islam et al., 2020; Su et al., 2019). Change in and/or depletion of O_2 levels at the cathode side could influence output power reproducibility. Hence, non-enzymatic catalysts should have high electrocatalytic performance and be selective to the glucose oxidation or oxygen reduction reactions.

Furthermore, most reported glucose fuel cells included a Nafion membrane as an ion transporter that maintains charge between the anodic and cathodic compartments. Nafion membranes are very expensive and are prone to clogging. There is, therefore, strong demand to develop membrane-less glucose-O_2 n-EFCs that can operate at a near-physiological pH and which are not dependent on the amount of dissolved oxygen. To date, only a few experimental data from blood, serum, or undiluted tissue fluid have been reported (Holade et al., 2014).

In this study, a new configuration of membrane-less glucose-O_2 n-EFCs based on air-

breathing cathode and non-enzymatic anode was constructed for the first time. The anode was a screen-printed carbon electrode (SPCE) modified with f-CNT and an electrodeposited PdAuNS. The cathode for Oxygen Reaction Reduction (ORR) was an air-breathing cathode composed of platinum/carbon (Pt/C)-coated carbon cloth with polytetrafluoroethylene (PTFE) layers as air diffusion layers. As far as we know, air cathodes were evaluated for the first time in this n-EFC technology. To optimize the electrocatalytic performance of the anode, the electrodeposition of the Pd and Au catalysts was studied in both monometallic and bimetallic configurations. The electrocatalytic activity of the electrodeposited catalysts was investigated for the direct glucose oxidation in neutral buffered solution. The effect of the metallic precursor concentrations on the morphology evolution of the electrodeposited nanostructures was investigated using scanning electron microscopy (SEM). The electrocatalytic activity of the catalysts towards glucose was characterized by cyclic voltammetry (CV) and linear sweep voltammetry (LSV). Structural, morphological, and electrochemical properties of PdAuNS coated SPCE anodes were studied for power generation in glucose-O_2 n-EFCs.

2. Experimental section

2.1.Chemicals and reagents

D-(+)-glucose (≥99.5%), tetrachloroauric (III) acid ($HAuCl_4.3H_2O$, ≥ 99.9), and palladium (II) chloride ($PdCl_2$, 59.8 wt.%) were obtained from Johnson Matthey (UK). Carboxylic acid functionalized multi-walled carbon nanotube (f-CNT), > 80% carbon basis, >8% carboxylic acid-functionalized, avg. D x L 9.5 nm x 1.5 µm, N,N-Dimethylformamide (DMF), Nafion (5 wt.%), sulfuric acid (H_2SO_4, 98%), polytetrafluoroethylene 60% wt. % / H_2O (PTFE), platinum on carbon, 10 wt. % Pt/C, and perchloric acid ($HClO_4$, 70.0-72.0%) were purchased from Sigma Aldrich (USA) and used as received without further purification. Carbon Black (CB) was purchased from Alfa Aesar. Carbon cloth (CC) (Fuel Cell Earth, USA). All other chemicals used in this work are of analytical reagent grade. 200 mM glucose stock solution was prepared in 0.1 M phosphate buffer solution (PBS) and stored at 4 °C. Glucose stock solution was allowed to mutarotate under magnetic stirring for at least 24 hours before use. The ultrapure water (18.2 $M\Omega.cm^{-2}$) was used to prepare all electrolytes. The electrochemical electrooxidation of glucose was done in 0.1 M PBS (pH 7.4), prepared using the analytical grade reagents, Na_2HPO_4 and KH_2PO_4 dissolved in distilled water, purchased from Solvachim (Morocco).

2.2.Apparatus and electrochemical techniques

CV, LSV, amperometry, and polarization/power curves were carried out at room temperature using a PalmSens potentiostat (BV Houten-Netherlands) connected to a computer and controlled by PSTrace5.8 software. The electrodeposition, polarization of metals catalysts, and the electrochemical behaviour of glucose were investigated using a conventional three-electrode electrochemical system. The working electrode (WE), counter electrode (CE), and reference electrode (RE) were an SPCE with a diameter of 3 mm, a stainless steel rod, and a saturated calomel electrode (SCE), saturated with 3M KCl, respectively. A 3D printer (Formlabs, US) was used specifically to print non-enzymatic fuel cell reactors in a 3D format. Schematics and engineering drawings for reactors construction were provided in the supplementary information (**Fig. S1**). The polarization and power curves were carried out in 0.1 M PBS (pH 7.4) containing glucose molecules. To avoid any kind of drop in resistance, the same two- or three-electrode system was used for all the electrochemical experiments in different electrolytic solutions, respecting approximately the same inter-electrode distances from one setup to another. The morphology of the as-prepared catalyst was investigated by field emission scanning electron microscopy (SEM) (SEM TESCAN model MIRA-3 (TESCAN-ORSAY, Brno, Czech Republic)).

2.3.Production of SPCE

Screen-printed carbon electrodes (SPCEs) were home-made with a 245 DEK (Weymouth, UK) screen-printing machine. Graphite-based ink (Electrodag 423 SS) from Acheson (Milan, Italy) was used to print the working and counter electrodes. The substrate was a flexible polyester film (Autostat HT5) obtained from Autotype Italia (Milan, Italy). The homemade electrodes were produced in foils of 48 units. The diameter of the working electrode was 3 mm, resulting in a geometric area of 0.07 cm^2. These electrodes were obtained as a gift from Professor Fabiana Arduini at Tor Vergata University (Rome, Italy).

2.4.Preparation of PdAuNS anodic catalyst modified SPCE

A simple process based on a flexible and rapid electrodeposition method was developed to elaborate the anodic catalyst. The f-CNT dispersion was prepared following the optimal method described in the previously reported protocol (Fan et al., 2011). Briefly, 10 mg of f-CNT nanoparticles were added into 10 mL of dispersing agent of 0.125 % (v/v) Nafion in DMF and sonicated for 3 h. 6 µL of as-prepared dispersion were drop casted in three steps of 2 µL over the WE surface of the SPCE. The f-CNT/SPCE is allowed to dry at 45 °C for 15

min after each casting step, resulting in a stable "film" of f-CNT formed on the electrode surface. With the help of a three-electrode system, electrodeposition of nanostructured anodic catalyst on the f-CNT/SPCE surface was performed at a fixed deposition potential (E_{dep} = -0.3 V vs. SCE) for 300 s in an acidic medium of 0.05 M $HClO_4$ and 0.25 M H_2SO_4 containing various concentrations of metallic precursor ($PdCl_2$ and/or $HAuCl_4$), resulting in the PdNS, AuNS, or PdAuNS/f-CNT/SPCE anodes. This applied potential value was chosen as the lowest negative value allowing the electrodeposition of both catalysts. Below -0.3 V vs. SCE, hydrogen evolution (electrochemical reduction of H^+ from the acidic medium) results in a detachment of f-CNTs from the electrode surface. However, the deposition time (t_{dep} = 300 s) was selected according to the previously reported study by (Zhao et al., 2019). Thereafter, a cyclic voltammetry mode in the range of -0.1–1.5 V vs. SCE was recorded for five successive cycles at a scan rate of 100 $mV.s^{-1}$ in 0.5 M H_2SO_4 to polarize the metal electrodeposited anodes. The electrochemical polarization helped to reach the oxide-rich surface and increased the electrochemical surface area through the formation of surface defects, atoms reordering, clusters of adatoms, etc (Grdeń et al., 2008). Finally, the anodic catalysts were rinsed and air-dried at room temperature before further electrochemical testing. It should be noted that a rinsing step was performed after electrodeposition and before the subsequent electrochemical tests. **Scheme 1a** shows the procedure for modifying the electrode surface with f-CNT dispersion and Pd and/or Au NS-based metallic catalyst through a simple electrodeposition method.

2.5.Preparation of Pt/C air cathode

Air cathodes are the most commonly used cathodes in microbial fuel cell (MFC) technology. A high power density of an air cathode MFC was achieved due to both the air cathode use and the elimination of the proton exchange membrane (PEM) (Liu and Logan, 2004). Air cathodes were fabricated following the previously reported protocol (Middaugh et al., 2006). **Scheme 1b** illustrates a brief process for producing air cathodes. Generally, they are composed of the carbon cloth (CC) as a current collector, the conductive carbon black (CB)-based gas diffusion layer, the PTFE diffusion layers, and the Pt/C-based catalyst layer. Firstly, a mixture of an appropriate ratio of CB powder and PTFE dispersion (19 µL of 40 % PTFE dispersion for each 1 mg CB per 1 cm^2 CC) was coated onto one side of CC with the help of a small paintbrush to produce a CB-based gas diffusion layer. Thereafter, four PTFE diffusion layers were applied by four successive coatings of the PTFE solution 60% (w/v). These were, afterward, heated for 30 min at 370 °C after each coating step. The as-prepared side of the CC

will be in contact with the air, thereby controlling the O_2 diffusion. Secondly, the other side of the Pt/C catalyst-based CC was prepared by pasting a vortexed mixture of 10% Pt/C, water, glass beads, Nafion (as a binder), and iso-propanol, which was subsequently allowed to air-dry for at least 24 h as previously detailed. The the air cathode was then ready for use.

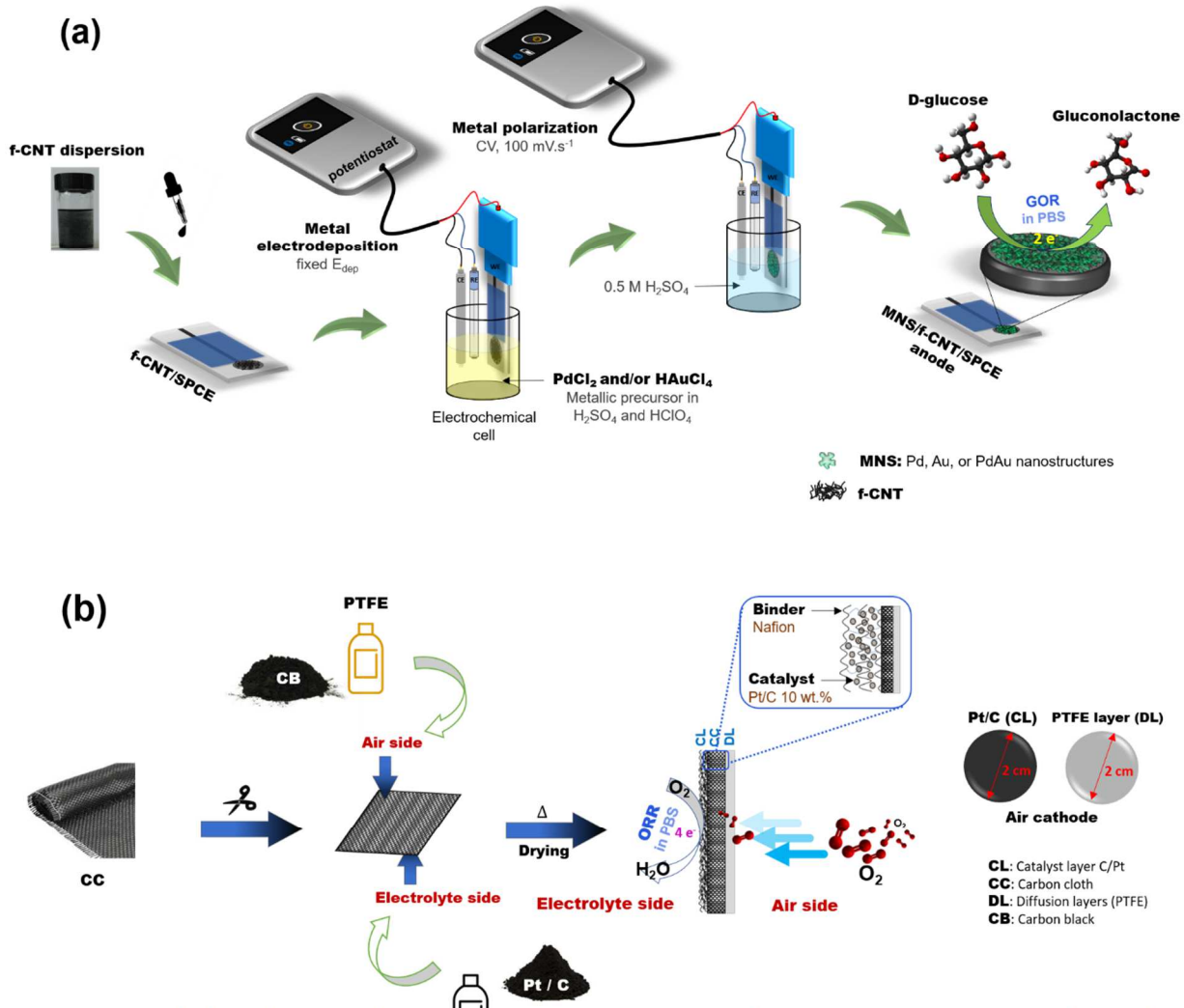

Scheme 1. Abiotic electrocatalyst based on **M** (Pd, Au, PdAu) NS for GOR and air-cathode based Pt/C catalyst for ORR in a neutral buffered solution (PBS, pH 7.4). **a)** Schematic illustration of the fabrication process of the non-enzymatic anodic catalyst starts with surface modification of the SPCE with f-CNT dispersion, then electrodeposition using chronoamperometry of metal catalyst (PdNS, AuNS, PdAuNS) in 0.05 M $HClO_4$ and 0.25 M H_2SO_4 solution containing metallic precursor. After electrodeposition, the three-electrode were rinsed and moved to another cell containing 0.5 M H_2SO_4 for polarization of **M**NS deposited anodes using CV prior to its utilization towards GOR. **b)** Schematic illustration of air-cathode production for the ORR in the proposed membrane-less neutral glucose/O_2 non-enzymatic fuel cell.

2.6.Design and set-up of the proposed non-enzymatic fuel cell

The compartment-less non-enzymatic fuel cell (n-EFC) was constructed with PdAuNS/f-CNT/SPCE anode and Pt/C loaded CC cathode. The single-chambered air cathode cylindrical-shaped n-EFC (2 cm long by 2 cm in diameter) was filled with 0.1 M PBS (pH 7.4) without any further air saturation (**Scheme S1**) and then operated to investigate the power density at various glucose concentrations. Using a PalmSens potentiostat, the Open Circuit Potential (OCP) was continuously monitored after assembling the n-EFC filled with 0.1 M PBS containing glucose. Once E_{OCP} has attained the steady-state, LSV measurements are subsequently recorded at 10 $mV.s^{-1}$ to obtain polarization and power density curves. Three replicates were carried out for each experiment. The currents and power densities were normalized versus the geometric surface of anodes.

2.7.Electrochemical analysis

Before the n-EFC assembling, it is fundamental to study the electrochemical behaviour of the anodic catalyst towards glucose in an electrochemical glucose sensor configuration. Firstly, CV measurements were carried out at a well-defined potential range positively scanned with a step potential of 8 mV, and conducted at a scan rate of 10 $mV.s^{-1}$ in 0.1 M PBS (pH 7.4) containing an appropriate amount of glucose. The analytical performance towards glucose electrooxidation under optimal conditions was carried out at PdNS, AuNS, and PdAuNS/f-CNT/SPCE anodes using amperometric batch analysis in 10 mL of stirred 0.1 M PBS (300 rpm) under a selected working potential. When a stable baseline current was reached, the glucose was added successively, and the amperometric responses were recorded. The anode providing the highest sensitivity towards glucose electrooxidation was selected as the anodic catalyst in an n-EFC configuration.

In an n-EFC configuration, the electrochemical performances of anode and cathode for glucose electrooxidation and oxygen electroreduction, respectively, in 0.1 M PBS are prerequisites to checking the current limiting electrode. Cathode and anode polarization curves were evaluated with LSV at 10 $mV.s^{-1}$ employing a potentiostat in a three-electrode electrochemical cell. The electrochemical cells were conventional and single-chambered air cathode cylindrical-shaped electrochemical cells. A Pt electrode (0.25 cm^2 immersed area) was used as CE and SCE as RE located close to the WE. For comparison study, Pt electrode and air cathode (2 cm in diameter) were tested as WEs toward oxygen electroreduction to evaluate the current limiting electrode.

3. Results and discussion

3.1.Electrochemical and morphological characterization of the f-CNT/SPCE

A comparative study of morphological structures and electrochemical performances of bare SPCE and f-CNT/SPCE was achieved. As shown in **Fig. S2**, the morphological characterization was investigated by SEM, showing the successful modification of the SPCE surface with f-CNT dispersion. The CV measurements performed in 0.1 M KCl solution containing 5 mM $[Fe(CN)_6]^{3-/4-}$ indicated that the presence of f-CNT improved the electron transfer significantly on the SPCE surface. Indeed, CVs showed a substantial decrease in the peak-to-peak separation (ΔEp), from a fully quasi-reversible system at bare SPCE with high ΔEp (534 mV) to a fast reversible system with lower ΔEp (115 mV), indicating that the fast electron transfer occurred at the f-CNT/SPCE (**Fig. S2**). The enhanced electron transfer, at f-CNT/SPCE, is probably due to the high electrical conductivity of CNT with a large surface-to-volume ratio, compared to the bare SPCE. These results are coherent with previously reported studies (T.-W. Chen et al., 2019; Meng et al., 2009). Therefore, f-CNTs were selected as supporting platform/material for coating SPCE in the rest of this work.

3.2.Electrocatalytic properties of monometallic AuNS and PdNS catalysts

3.2.1. Morphological characterization of deposited AuNS and PdNS

The metallic precursor concentration is an essential parameter for controlling the morphological structures of electrodeposited catalysts. Both PdNS and AuNS were separately electrodeposited by chronoamperometry at fixed deposition potential (E_{dep} = -0.3 V vs. SCE) for 300 s in a 0.05 M $HClO_4$ and 0.25 M H_2SO_4 solution containing various concentrations of metallic precursor ($PdCl_2$, $HAuCl_4$). The as-deposited AuNS and PdNS on f-CNT/SPCE were then electrochemically polarized in 0.5 M H_2SO_4 solution for five successive cycles using CV in the potential range of -0.2 V to 1.5 V vs. SCE at a scan rate of 100 $mV.s^{-1}$.

The morphology evolution of electrodeposited PdNS and AuNS on f-CNT/SPCEs was investigated by SEM as a function of the metallic precursor concentration. **Fig. 1** shows typical SEM images of PdNS and AuNS, illustrating the structure shape evolution of electrodeposited metallic nanostructures (**Fig. 1a** to **Fig. 1d** for PdNS and

Fig. 1e to **Fig. 1h** for AuNS), in which the pairs **a-e**, **b-f**, **c-g**, and **d-h** correspond to the ion metal concentrations of 10, 20, 50, and 100 mM, respectively. It could be observed that the morphology of nanostructured Pd and Au deposited onto f-CNT/SPCE changed considerably with the precursor concentration during electrodeposition. SEM characterization was, indeed, used to investigate the effect of precursor solution concentration on the morphology of electrodeposited Pd and Au nanostructures. By increasing the precursor concentration, the Pd structure changed from microclusters to 3D cauliflower-like microstructured porous Pd. However, Au structure changed from dendrite-like microstructured porous Au to sheet-like Au microstructures. Using 10 mM $PdCl_2$ (**Fig. 1a**), the morphology of Pd was cluster-shaped microstructures until they get bigger and bigger when 20 mM (**Fig. 1b**) to 50 mM (**Fig. 1c**) $PdCl_2$ were used during the electrodeposition process. Up to 100 mM $PdCl_2$ resulted in dense and large cauliflower-shaped structured Pd with a large electrocatalytic surface area on the f-CNT/SPCE surface, as shown in **Fig. 1d**. These results demonstrate that the precursor concentration has a crucial effect on the control of Pd structure morphology and supply more catalytic sites to benefit the electrocatalytic oxidation of glucose molecules. Regarding the Au catalyst, with increasing the $HAuCl_4$ concentration from 10 mM to 50 mM, the loading of dendrite-like Au structures increased on the surface of the f-CNT/SPCE. However, above this range, the deposited AuNS took the form of sheet-like Au structures.

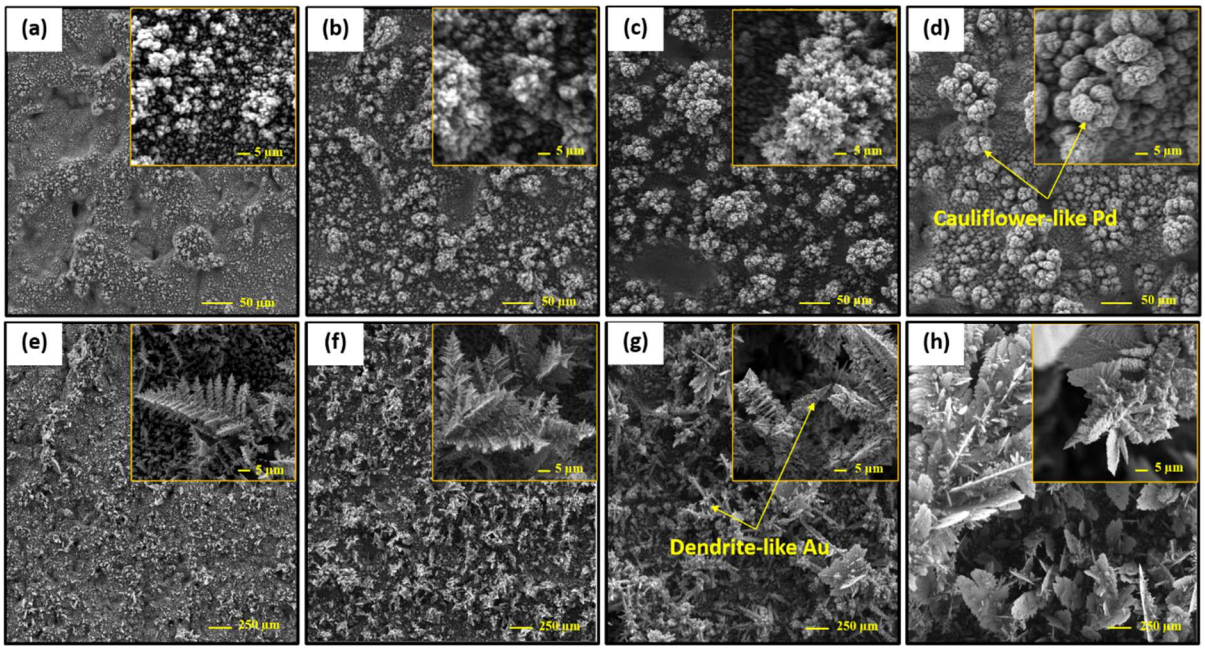

Fig.1. SEM images: Shape evolution of deposited metals (**a** to **d** for PdNS and **e** to **h** for AuNS) as a function of metal precursor concentration, where the pairs **a-e**, **b-f**, **c-g**, and **d-h** correspond to the concentrations of 10, 20, 50, and 100 mM, respectively. The electrochemical deposition of AuNS and PdNS on the f-CNT/SPCE surface was performed in 0.05 M $HClO_4$ and 0.25 M H_2SO_4 solution containing various metallic precursor concentrations for 300 s at a constant deposition potential of -0.3 V vs. SCE.

3.2.2. Electrochemical behaviour of PdNS and AuNS towards glucose electrooxidation

The electrochemical behaviour of as-synthesized PdNS and AuNS towards glucose electrooxidation was assessed and discussed separately.

The electrochemical polarization of electrodeposited metal in acidic medium by the CV is an important step, which reveals the electrochemical behaviour of metallic catalyst. **Fig. 2A** and **Fig. 2B** show the first cycle after polarization cycling corresponding to typical CVs, as a function of metal precursor concentration, of PdNS and AuNS, respectively. Indeed, PdNS have shown the highest background current compared to AuNS, indicating that the slower charge transfer has occurred at Pd/f-CNT.

The Electrochemical surface area (ESA) of electrodeposited catalysts on electrodes was estimated by measuring the charge consumed (Q_{os}) during the electroreduction of Pd and Au oxides at the cathodic scan. This method was previously reported and was based on the assumption that the charge densities required to reduce a monolayer of

metallic oxides per unit surface area were 0.424 mC.cm^{-2} and 0.559 mC.cm^{-2} for PdO and Au_2O_3, respectively (Grdeń et al., 2008; Rand and Woods, 1971). The ESA value can be calculated according to the reported equation (Shu et al., 2014), equation 1.

$$ESA = \frac{Q_O}{Q_{OS}} \quad \left(Q_O = \frac{S}{V}\right) \qquad \textbf{(1)}$$

Where Q_o represents the charge required for oxygen adsorption, Q_{os} is the charge density required to reduce a monolayer of oxygen, S is the integral discharge area under the cathodic reduction peak, and V is the scan rate (100 mV.s^{-1}).

The ESA values of Pd catalyst obtained at various concentrations of 10, 20, 50, and 100 mM $PdCl_2$ were 3.93, 9.41, 19.50, and 47.71 cm^2, respectively. These results indicated that the ESA of PdNS-based f-CNT/SPCE increased significantly with precursor concentration. This can be due to the formation of cauliflower-like Pd nanostructures. However, the ESA values related to AuNS-based f-CNT/SPCE were 0.78, 1.75, 3.77, and 1.94 cm^2 using 10, 20, 50, and 100 mM $HAuCl_4$, respectively. Indeed, the ESA of AuNS deposited f-CNT/SPCE increased when the range 10–50 mM $HAuCl_4$ was used. Whereas, at 100 mM, the ESA decreased dramatically. This is probably due to a lower specific surface area of the sheet-like Au structures obtained at 100 mM $HAuCl_4$ concentration.

After electrodeposition of PdNS and AuNS and subsequent polarization cycling, measurements of LSV at 10 mV.s^{-1} and amperometry under an applied potential of +0.3 V vs. SCE were performed to investigate the electrocatalytic activities of PdNS/f-CNT/SPCE and AuNS/f-CNT/SPCE towards glucose electrooxidation in 0.1 M PBS. **Fig. 2C** and **Fig. 2D** show the LSV responses related to glucose oxidation recorded separately in 0.1 M PBS containing 20 mM glucose at PdNS/f-CNT/SPCE and AuNS/f-CNT/SPCE, respectively. As can be seen in **Fig. 2C**, the electrocatalytic activity of PdNS/f-CNT/SPCE towards glucose oxidation increased with precursor concentration. Firstly, an oxidation peak was seen at around -0.4 V vs. SCE at PdNS/f-CNT/SPCE, its current intensity increased significantly with precursor concentration. This may be due to both desorption of H from the surface of PdNS catalyst via electrooxidation of Pd_2H (Pourbaix, 1974) and the dehydrogenation of glucose molecules via their adsorption onto the Pd catalyst (Li and Du, 2017). Secondly, a significant enhancement in the faradic current on the Pd electrocatalyst towards

glucose oxidation was observed at around +0.3 V vs. SCE. Furthermore, increasing the $PdCl_2$ precursor concentration from 10 to 100 mM resulted in a shift of the glucose oxidation peak towards positive potential values (from 165 to 300 mV vs. SCE).

On the other hand, **Fig. 2D** shows that AuNS was catalytically active to direct glucose electrooxidation in the potential range of -0.1 to +0.3 V vs. SCE and the $HAuCl_4$ precursor concentration range from 10 to 50 mM. Up to 100 mM, the electrocatalytic activity of AuNS/f-CNT/SPCE decreased significantly, which may be due to the fact that the 2D sheet-like Au structure possesses a low catalytic ESA compared to the dendrite-like ones. Unlike PdNS/f-CNT/SPCE, the glucose oxidation peak on AuNS/f-CNT/SPCE showed a negative shift in peak potential from 270 to -110 mV vs. SCE with increasing $HAuCl_4$ precursor concentration from 10 to 100 mM.

Fig. 2E and **Fig. 2F** show amperometric responses obtained at PdNS/f-CNT/SPCE and AuNS/f-CNT/SPCE, respectively, with a successive glucose addition of 1 to 20 mM in 0.1 M PBS (pH 7.4). As can be seen in amperometry plots, the AuNS/f-CNT catalyst has provided the highest faradic current against glucose electrooxidation compared to the PdNS/f-CNT catalyst. The amperometric responses presented a good linear relationship with glucose concentration between 1 and 41 mM on both electrodes, as indicated in **Table S1**. The sensitivity and Limit of Detection (LOD) were significantly improved at PdNS catalyst by increasing the $PdCl_2$ precursor concentration from 10 to 100 mM. However, at AuNS-based electrochemical anodes, the analytical performances dropped dramatically, as 100 mM of metal precursor was used. The results obtained by the amperometry are coherent with those obtained by using LSV. **Table S1** summarizes the analytical parameters provided by amperometry at PdNS/f-CNT/SPCE and AuNS/f-CNT/SPCE under +0.3 V vs. SCE. Importantly, the AuNS/f-CNT/SPCE electrode showed excellent sensitivity with a lower LOD in the $HAuCl_4$ precursor concentration range of 10–50 mM, compared to 10–100 mM for PdNS/f-CNT/SPCE construction. It was also observed that ESA values and electrocatalytic activities towards glucose electrooxidation obtained for both AuNS and PdNS modified f-CNT/SPCE are coherent with the morphological structure evolution observed in the SEM images (**Fig. 1**).

Consequently, the results above demonstrated that the maximum electrocatalytic activities of the PdNS/f-CNT/SPCE and AuNS/f-CNT/SPCE towards glucose electrooxidation were obtained for metallic precursor concentrations of 100 mM and

50 mM, respectively. Therefore, they were chosen as optimal, offering high sensitivities, low LODs, as well as cauliflower- and dendrites-like 3D porous nanostructures for Pd and Au, respectively.

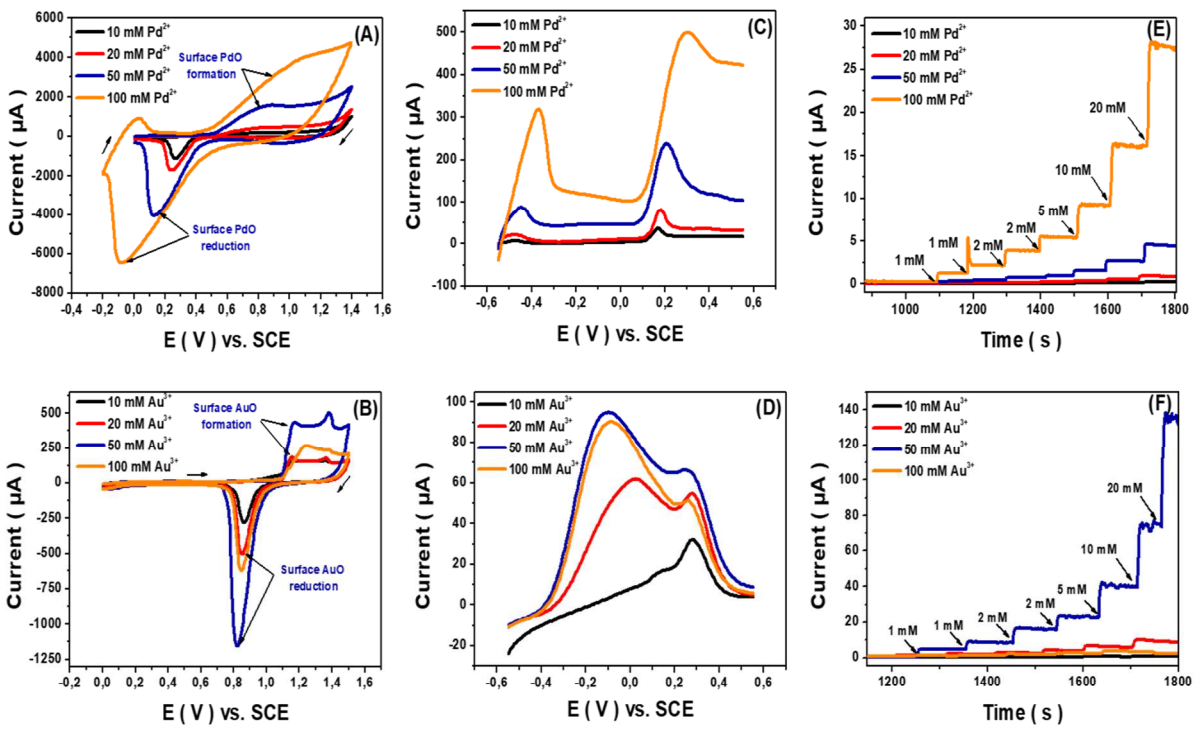

Fig.2. 1st cycle, of five successive cycles, related to the polarization of **A)** PdNS- and **B)** AuNS-deposited f-CNT/SPCE recorded by CV in 0.5 M H_2SO_4 solution, scan rate 100 mV.s^{-1}. LSVs recorded **C)** PdNS/f-CNT/SPCE and at **D)** AuNS/f-CNT/SPCE of 0.1 M PBS (pH 7.4) containing 20 mM glucose, scan rate 10 mV.s^{-1}. Amperogramms at **E)** PdNS/f-CNT/SPCE and at **F)** AuNS/f-CNT/SPCE in the glucose concentration range of 1–20 mM in 0.1 M PBS at a fixed potential of +0.3 V vs. SCE. All LSVs and amperograms were recorded after the electrodeposition of PdNS and AuNS under -0.3 V vs. SCE for 300 s in a 0.05 M $HClO_4$ and 0.25 M H_2SO_4 solution containing various concentrations of $HAuCl_4$ or $PdCl_2$ (10, 20, 50, 100 mM) followed by their polarization in 0.5 M H_2SO_4 using CV.

3.2.3. Stability study of the glucose electrochemical response

The stability of the electrochemical response of glucose electrooxidation was investigated separately at PdNS/f-CNT/SPCE and AuNS/f-CNT/SPCE anodes using LSV at 10 mV.s^{-1} and amperometric measurements recorded at a potential value of +0.3 V vs. SCE. **Fig. S3A** and **Fig. S3B** showed the electrochemical behaviour of both metallic catalysts modified f-CNT/SPCE towards glucose electrooxidation reaction (GOR) in 0.1 M PBS containing 20

mM glucose using LSV in the potential range of -0.55 to +0.6 V vs. SCE. As shown in **Fig. S3A**, the electrochemical response corresponding to GOR at AuNS/f-CNT/SPCE decreased after the first anodic measurement. This result was congruent with that displayed in **Fig. S3C**, where the amperometric response was unstable each time glucose was added to the buffer solution. This issue could be attributed to the fact that there is high adsorption of glucose oxidation products, a process which further blocks the access of glucose molecules to catalytic sites and consequently affects the response's lifespan of the electrocatalyst. In contrast, the signal obtained at PdNS/f-CNT/SPCE remained largely stable during LSV measurements for two consecutive scans against 20 mM glucose (**Fig. S3B**) and during amperometric measurements following sequential glucose additions (**Fig. S3D**). Furthermore, the sensitivity obtained on AuNS/f-CNT/SPCE tends to decrease in high glucose concentrations compared to that found on PdNS/f-CNT/SPCE (as shown in the insert **Fig. S3C** and the insert **Fig. S3D**). Nevertheless, it should be noted that AuNS/f-CNT/SPCE provided the lowest LOD of 170 µM compared to 702 µM obtained on PdNS/f-CNT/SPCE based on S/N = 3.

Therefore, both catalysts showed interesting characteristics. Au showed better sensitivity and LOD while Pd displayed improved stability towards glucose electrooxidation signal. Thus, taking advantage of each pure metal catalyst's properties, a binary catalyst system would be of great interest to show the synergistic effect of Pd and Au catalysts toward GOR.

3.3.Electrocatalytic properties of bimetallic PdAuNS catalyst

As demonstrated above in **Fig. 2**, the AuNS catalyst offered the highest sensitivity and the lowest LOD towards glucose electrooxidation. However, the PdNS catalyst showed its poison tolerance to GOR products and good linearity over the whole concentration range of the $PdCl_2$ metallic precursor, whereas Au was extremely susceptible to fouling. Each metal catalyst, therefore, holds specific advantages towards the GOR. Indeed Pd and Au precursors were mixed in one solution containing various Pd:Au ratios of the previously optimized metallic precursor concentrations (50 mM $HAuCl_4$ and 100 mM $PdCl_2$). These precursor solutions were used for further electrochemical co-deposition via chronoamperometry at -0.3 V vs. SCE, as shown in **Fig. 3A**. As displayed in **Fig. 3B**, the co-deposited alloy PdAuNS on f-CNT/SPCE was then polarized using CV (see also the separate polarization CVs in **Fig. S4**). The electrochemical behaviour of Pd-Au bimetallic catalyst obtained at different concentration ratios of their precursors was investigated. The SEM analysis was used to evaluate the structure shape evolution of co-deposited PdAuNS as a function of their metal

precursor ratio, **Fig. S4**. Consequently, a Pd-Au bimetallic mixture of cauliflower- and dendrite-like 3D porous nanostructures was found.

As shown in **Fig. 3C**, the electrocatalytic activity of PdAuNS anodes towards GOR was assessed in 0.1 M PBS by amperometry at +0.3 V vs. SCE, indicating their electrochemical responses after successive glucose addition. **Fig. 3D** illustrates the corresponding calibration curves, revealing a wide linear regression between the anodic currents and the glucose concentration. As a consequence, the bimetallic precursor Pd/Au with the 1 : 1 volume ratio shows excellent analytical performance, including a high sensitivity of 126.78 ± 12.85 $\mu A.mM^{-1}.cm^{-2}$ with RSD % of 10.90 and a low LOD of 14 µM (S/N = 3), **Fig. 3E**. Furthermore, PdAuNS binary system proposed in this work demonstrated better catalytic performance towards GOR with faster kinetics than individual metals. The enhanced electrocatalytic activity can be attributed to the strong synergistic effect of the bimetallic system Pd-Au. This effect makes it easier for glucose to bind to the electrode surface, as glucose can be electrochemically adsorbed faster onto Au catalytic sites by dehydrogenation (Pasta et al., 2010). After that, dehydrogenated glucose is oxidized to gluconolactone by both catalysts (Li and Du, 2017). Besides, a stability study of the amperometric signal towards electrooxidation of 5 mM glucose was conducted on both individual metals (Pd, Au) and their combination Pd-Au. **Fig. 3F** shows the amperometric signal decrease of glucose electrooxidation at PdNS, AuNS, and Pd-AuNS catalysts after 45 minutes of glucose addition. Improved signal stability was achieved when both metal catalysts were used in combination. This record performance was attributed to the synergistic contribution of PdNS, AuNS, and f-CNT. Analytical performances of the developed non-enzymatic catalyst were compared with other non-enzymatic anodes towards GOR in neutral and alkaline environments, as listed in **Table S2**. Analytical features of the developed PdAuNS/f-CNT catalyst are comparable to those in reported works. Benefitting from the excellent performance towards GOR, the developed non-enzymatic catalyst was selected as anode material for glucose fuel cell application.

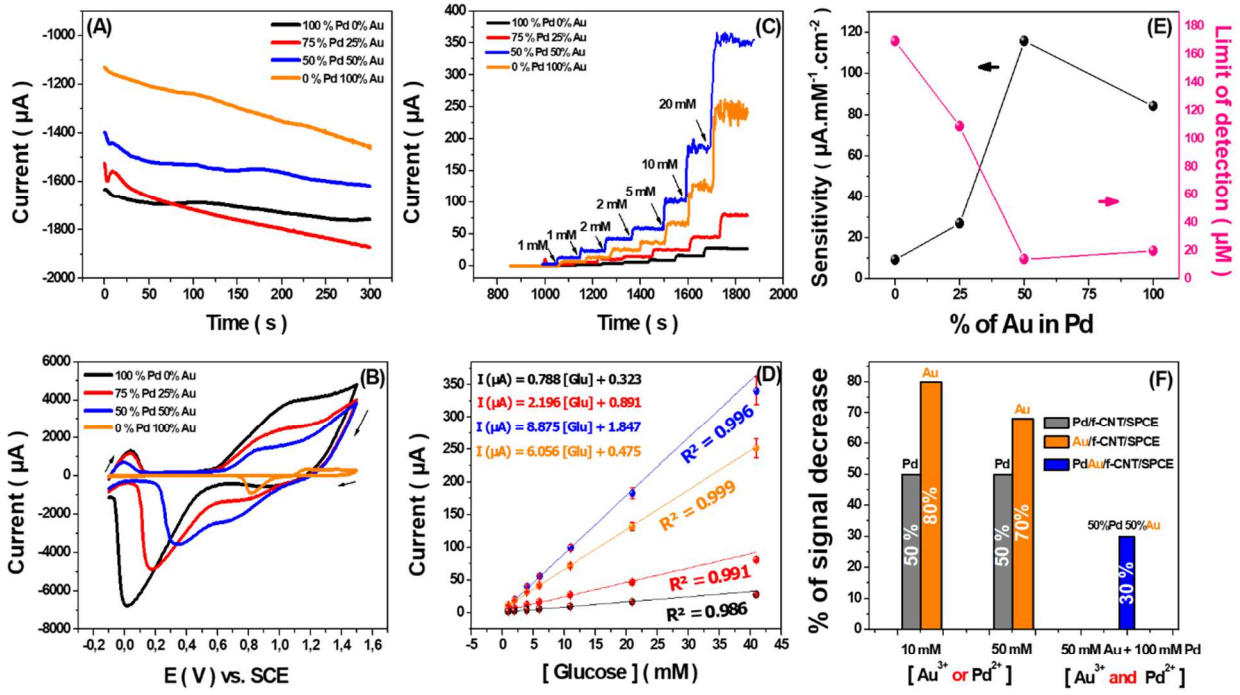

Fig.3. A) Chronoamperograms related to PdAuNS electrochemical co-deposition under -0.3 V vs. SCE for 300 s in a solution of 0.05 M $HClO_4$ and 0.25 M H_2SO_4 containing various concentration ratios of $PdCl_2$ and $HAuCl_4$. **B)** Polarization of the deposited alloy, Pd-Au, using CV in 0.5 M H_2SO_4, scan rate 100 $mV.s^{-1}$. **C)** Amperometric responses under +0.3 V vs. SCE of $Au_{(x-1)}Pd_xNS$/f-CNT/SPCE towards successive addition of glucose in 0.1 M PBS and **D)** their corresponding calibration curves. **E)** Effect of Pd:Au ratios on analytical performances of the anode towards GOR. **F)** Statistical graph illustrating the amperometric signal decrease related to the electrooxidation of 5 mM glucose at each catalyst alone (Pd or Au) and its PdAu alloy.

3.4.Electrocatalytic performance of solid platinum and air cathode as cathode materials

The electrochemical performance of the cathode towards oxygen reduction reaction (ORR) is crucial before such a glucose/O_2 non-enzymatic fuel cell (n-EFC) operation. The electrical performances of the fuel cell are significantly related to the cathode. Furthermore, in many reported studies (**Table 1**), the lower output signal (power, current density) of glucose/O_2 n-EFC could be limited by the dissolved O_2 due to its low concentration. Hence, to attain the highest electrical performances, the enhancement of the O_2 concentration and the cathode material are two critical parameters that should be considered.

Two kinds of cathodes were selected to gain insight into the ORR as well as the current limiting electrode concept: a conventional platinum electrode and a Pt/C/Nafion coated carbon cloth air-breathing cathode. In this context, three-electrode systems based on a conventional electrochemical cell and a single-chambered air cathode cylindrical-shaped were constructed and assembled. As shown in **Fig. S5**, the polarization curves of anode and cathode were evaluated separately for glucose oxidation and oxygen reduction in 0.1 M PBS using LSV at 10 $mV.s^{-1}$. In both configurations, a Pt electrode (0.25 cm^2 immersed area) was used as CE, a PdAuNS/f-CNT/SPCE as WE (anode) for glucose oxidation, and a SCE as RE. However, a Pt cathode and air cathode (2 cm in diameter) were used for ORR as WEs. Unlike the air cathode, ORR on the conventional Pt cathode requires O_2-saturated 0.1 M PBS. Compared with the conventional Pt electrode, it was found that a high electrocatalytic activity for ORR, with a low overpotential, was clearly observed for Pt/C air-breathing cathode without any further air-saturation. Therefore, air cathodes would be a suitable catalyst for ORR in a glucose/O_2 n-EFC configuration employing oxygen from the air to enhance both diffusivity and oxygen concentration.

3.5.Performances of the air-breathing cathode glucose/O_2 fuel cell

As mentioned above, the obtained results demonstrate the outstanding electrocatalytic activity of PdAuNS/f-CNT/SPCE anode and air-breathing cathode towards direct GOR and ORR, respectively. A new architecture of a membrane-less single chamber n-EFC device (**Fig. 4A**) was, therefore, constructed using PdAuNS/f-CNT/SPCE as an anodic catalyst and air-breathing cathode as a cathodic catalyst. Both electrodes were then assembled in the n-EFC device, filled with 0.1 M PBS. As shown in **Fig. 4A**, it can be assumed that glucose first undergoes adsorption on the surface of the anodic catalyst and then directly oxidized catalytically to gluconolactone, producing electrons and protons. The electrons move to the cathode via the external circuit connecting both electrodes. Simultaneously, protons easily reach the cathode through the supporting electrolyte without any use of a proton exchange membrane (PEMs). In this spontaneous process, glucose is used as fuel to produce electricity. The redox reactions of the proposed glucose/O_2 n-EFC are as follows:

Anode : $C_6H_{12}O_6$ (glucose) $\xrightarrow{PdAu}$ $C_6H_{10}O_6$ (gluconolactone) + $2H^+ + 2e^-$

Cathode : $O_2 + 4H^+ + 4e^- \xrightarrow{Pt/C} 2H_2O$

Total : $C_6H_{12}O_6$ (glucose) + $1/2O_2$ ⟶ $C_6H_{10}O_6$ (gluconolactone) + H_2O

Fig. 4B shows the change in Open Circuit Potential (OCP) as a function of glucose concentration, depicting that the OCP becomes larger up to 10 mM and stabilizes after this value. The OCP variations vs. SCE at the cathode and the anode with increasing glucose concentration were also investigated, as shown in **Fig. 4C**. Compared to the anode, the cathode potential varies slightly with glucose concentration, indicating that the anode catalyst has excellent electrocatalytic activity towards glucose. Hence, even with the membrane-less device, the cathode is not affected by the presence of glucose molecules. Moreover, **Fig. 4D** shows the polarization and power curves of the abiotic glucose/O_2 fuel cell at different glucose concentrations. A sudden drop can be seen in current/power densities during direct polarization tests of the anodic potential. This drop could be attributed to the fact that once an anodic potential allowing glucose oxidation was reached, a strong/fast desorption phenomenon of protons from the Pd-Au catalyst (during glucose dehydrogenation) probably takes place (Li and Du, 2017). The maximum power density (P_{max}) presents a good linear relationship with glucose concentration between 1 and 20 mM, as illustrated in **Fig. 4E**. The limit of detection (LOD) was calculated to be 0.3 mM. This could lead to an intriguing idea for developing more advanced self-powered sensing technology for on-site biomedical diagnosis and environmental monitoring using a simple galvanic cell design. Additionally, electrical characterization of the glucose/O_2 n-EFC supplied with a neutral buffered solution containing 20 mM glucose showed a maximal power output of 129 ± 11 $\mu W.cm^{-2}$, a current density of 600 ± 39 $\mu A.cm^{-2}$ with a cell voltage of 0.35 V and an OCP of 0.56 V. Moreover, the polarization resistance contribution of PdAu anode and Pt/C air-breathing cathode was given as a function of glucose concentration and was described in **Table S3**. Compared with other n-EFC (**Table 1**), the power value obtained in neutral media is relatively higher than that reported in most published studies. This can be attributed to removing the proton exchange membrane, enhancing the O_2 concentration, and controlling oxygen diffusivity using air-cathode technologies. Moreover, the proposed electrocatalyst possesses several advantages: fast response, low cost, poison-free characteristics, and good reproducibility. Thus, glucose/O_2 n-EFC could be of great interest in direct glucose fuel cell applications (e.g., powering mountable or implantable biomedical and environmental micro-devices running at low electrical power) or in self-powered sensing.

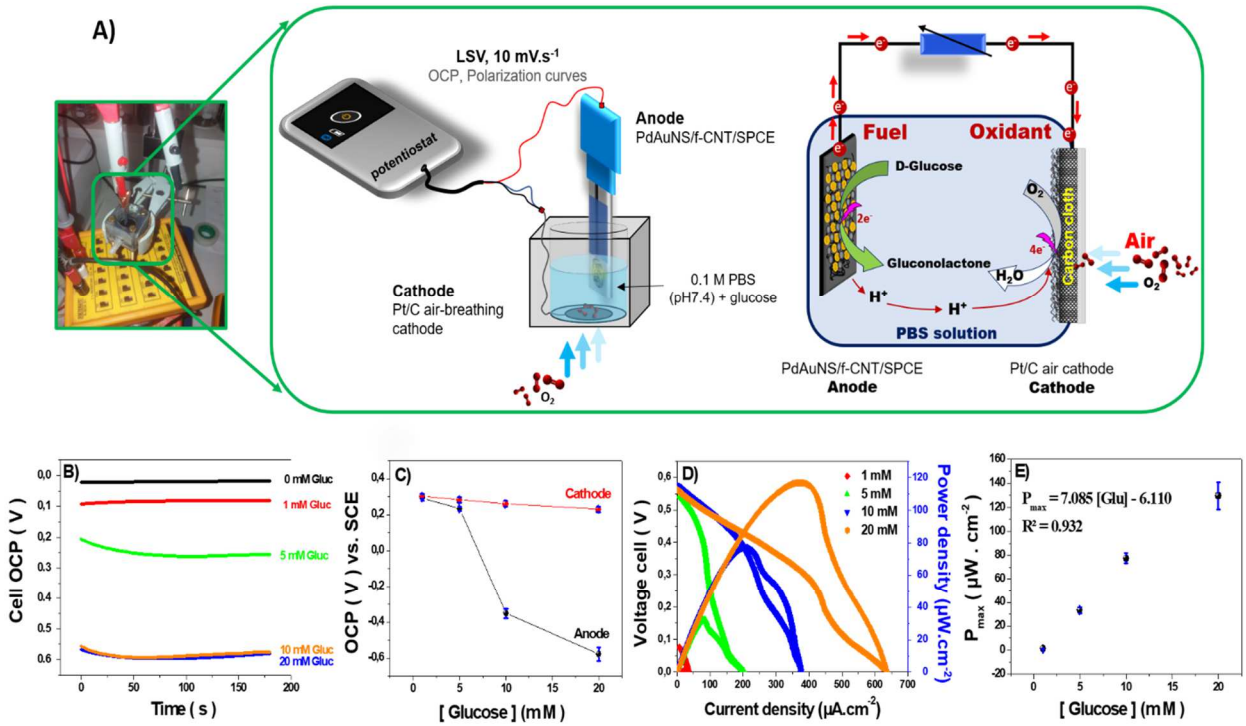

Fig. 4. A) Photo and schematic representations of the membrane-less glucose/O_2 n-EFC equipped with a PdAuNS/f-CNT/SPCE anode and an air cathode, highlighting the electrocatalytic oxidation/reduction reactions that take place in 0.1 M PBS (pH 7.4). **B**) OCP curves, **C)** OCP variation vs. SCE at the cathode and anode as a function of glucose concentration. **D)** Polarization and power density curves at different concentrations of glucose (1, 5, 10, 20 mM) in 0.1 M PBS, pH 7.4 and **E)** Calibration plot of power density output as a function of glucose concentration (1–20 mM) in glucose/O_2 n-EFC.

728

729

730

Table 1. Summary of analytical features of recently developed non-enzymatic glucose/O_2 fuel cells operated in a neutral and alkaline environment.

Anode catalyst	Cathode catalyst	Device configuration	OCP (V)	J_{SC} ($mA.cm^{-2}$)	Power density ($\mu A.cm^{-2}$)	Electrolyte + fuel concentration	Ref.
Pt/Au nano-alloy/Pt@PETE	graphene-modified GCE	With membrane	0.42	2.67	320	0.1 M PBS* + 5 mM glucose	(Chu et al., 2021)
Pouros Pt	Carbon nanohorns	With membrane	0.37	0.02	8.64	0.1 M PBS* + 30 mM glucose	(Islam et al., 2020)
AuNWs/GCE	Pt/C catalyst /GCE	With membrane	0.42	1.34	126	0.1 M PBS* + 30 mM glucose	(Yang et al., 2014)
Activated Pt	SWCNT network	With membrane	0.19	0.18	3.40	0.01 M PBS* + 10 mM glucose	(Rapoport et al., 2012)
PtPd/GO/SPE	NGONR/SPE	With membrane	0.22	0.10	8.96	0.01 M CSF* + 4 mM glucose	(Su et al., 2019)
PdPtAu/C	Activated charcoal	With membrane	0.92	-	520	1 M KOH* + 300 mM glucose	(Basu and Basu, 2012)
$Au_{80}Pt_{20}$-NPs/CB/carbon paper	PtNPs/CB/buckypaper	Membrane-less	0.36	1.30	182	0.2 M PBS* + orange	(Holade et al., 2015)
AuAg/MWCNT Au/MWCNT	Pt/C@PMMA plate	Membrane-less	0.83 0.58	9.50 5.80	1600 1040	0.3 M KOH + 10 mM glucose	(Arjona et al., 2015)
Pt/CNT	Pt/CNT	Membrane-less	0.27	11.00	0.77	0.1 M PBS + 500 mM glucose	(Ryu et al., 2010)
Co_3O_4-3DrGO/Nif	N,Fe-PSAC	Membrane-less	0.44	0.11	12.81	0.1 M KOH* + 10 mM glucose	(Purkait and Dey, 2020)
AuPd/C/GCE	Pt/C/GCE	Membrane-less	0.52	2.00	280	0.3 M KOH* + 10 mM glucose	(Arjona et al., 2014)
PdAuNS/f-CNT/SPCE	Pt/C/Air-breathing cathode	Membrane-less	0.56	0.60± 0.04	129 ± 11	0.1 M PBS + 20 mM glucose	**This work**

GCE: Glassy carbon electrode, **SPE:** Screen-printed electrode, **Pt@PETE:** Thin Pt layer coated polyethylene terephthalate membrane, **AuNWs/GCE:** Au nanowires modified GCE, **PtPd/G/SPE**: SPE modified with bimetallic PtPd nanocatalyst grafted graphene oxide, **NGONR/SPE**: Nitrogen-doped GO nanoribbons modified SPE, **CSF**: Neutral cerebrospinal fluid, **PdPtAu/C**: Carbon supported trimetallic PdPtAu nanoparticles, **CB**: Carbon black, **Pt/C@PMMA plate**: Pt/C modified poly(methyl methacrylate) plate, **Co_3O_4-3DrGO/Nif** : Nickel foam substrate modified with Co_3O_4 nanoparticles supported on 3D rGO networks, **N,Fe-PSAC**: Nitrogen and iron doped activated carbon material.
(*) referred to an O_2-saturated environment
J_{SC} indicated short-circuit current density

731

732 4. Conclusions

733

734 In summary, the porous cauliflowers-like PdAuNS were successfully prepared through
735 a cost-effective and straightforward electrodeposition method on the f-CNT/SPCE
736 surface. A highly sensitive electrochemical anode was developed for the direct

catalytic oxidation of glucose in neutral buffered solution (pH 7.4). Owing to their synergistic effect, the co-electrodeposited PdAuNS exhibited an excellent electrocatalytic activity for glucose oxidation. The PdAuNS anode that provides the highest sensitivity towards glucose electrooxidation was utilized to set up a new single-chambered non-enzymatic glucose-O_2 fuel cell based on an air-breathing cathode. Indeed, the integration of air cathodes in n-EFC technology has been evaluated for the first time. These cathodes are of particular interest since the glucose-O_2 n-EFCs do not require any further air bubbling or air-saturating conditions to operate. The n-EFCs obtained were able to yield stable power density as a function of glucose concentration with a high maximum power density. Despite these advantages, the soft nature of the PdAuNS/f-CNT electrocatalyst at the electrode surface may lead to a short lifespan as well as a decrease in catalytic activity due to the scratching of the surface. Hence, doping PdAuNS/f-CNT into highly stable and conductive matrices could enhance their attachment to the electrode surface.

The new n-EFC configuration combined with the proposed catalysts employed at the surface of both electrodes might be a potential alternative to the conventional enzymatic fuel cell for direct glucose fuel cell applications (e.g., a new electrochemical system that can supply mountable or implantable biomedical devices running at low electrical power such as pacemakers, artificial hearts, insulin pumps, etc.) or for self-powered sensors.

Acknowledgments: The authors greatly acknowledge the financial support of funding from the ‘‘Hubert Curien Program’’ through the PHC MAGHREB Project N°19MAG23/41382WC.

Conflict of interest: The authors declare that there is no conflict of interest.

5. References

Adeel, M., Rahman, M.M., Caligiuri, I., Canzonieri, V., Rizzolio, F., Daniele, S., 2020. Biosens. Bioelectron. 165, 112331.

Antolini, E., 2021. Energy Fuels 5, 5038–5060.

Aoun, S.B., Bang, G.S., Koga, T., Nonaka, Y., Sotomura, T., Taniguchi, I., 2003. Electrochem. Commun. 5, 317–320.

Arjona, N., Armenta-Gonzalez, A.J., Rivas, S., Guerra-Balcazar, M., Ledesma-Garcia, J., Arriaga, L.G., 2015. Energy 40, 14699–14705.

Arjona, N., Dector, A., Guerra-Balcázar, M., Álvarez-Contreras, L., Sabaté, N., Esquivel, J.P., Ledesma-García, J., Arriaga, L.G., 2014. RSC Adv. 4, 26158–26165.

Basu, D., Basu, S., 2012. Int. J. Hydrog. Energy 37, 4678–4684.

Brouzgou, A., Tsiakaras, P., 2015. Top. Catal. 58, 1311–1327.

Cadet, M., Gounel, S., Stines-Chaumeil, C., Brilland, X., Rouhana, J., Louerat, F., Mano, N., 2016. Biosens. Bioelectron. 83, 60–67.

Chansaenpak, K., Kamkaew, A., Lisnund, S., Prachai, P., Ratwirunkit, P., Jingpho, T., Blay, V., Pinyou, P., 2021. Biosensors 11, 16.

Chen, T.-W., Rajaji, U., Chen, S.-M., Muthumariyappan, A., Al Mogren, M.M., Ramalingam, R.J., Hochlaf, M., 2019. Ultrason. Sonochem. 58, 104596.

Chen, Y., Ji, W., Yan, K., Gao, J., Zhang, J., 2019. Nano Energy 61, 173–193.

Chu, M., Zhang, Y., Yang, L., Tan, Y., Deng, W., Ma, M., Su, X., Xie, Q., Yao, S., 2013. Energy Environ. Sci. 6, 3600–3604.

Chu, T.-F., Lin, F.-Y., Kuznetsova, I., Wang, G.-J., 2021. J. Power Sources 486, 229374.

Chu, T.-F., Rajendran, R., Kuznetsova, I., Wang, G.-J., 2020. J. Power Sources 453, 227844.

Cosnier, S., Gross, A.J., Le Goff, A., Holzinger, M., 2016. J. Power Sources 325, 252–263.

Cosnier, S., Le Goff, A., Holzinger, M., 2014. Electrochem. Commun. 38, 19–23.

Dutta, S., Patil, R., Dey, T., 2022. Nano Energy 107074.

Elouarzaki, K., Holzinger, M., Le Goff, A., Thery, J., Marks, R.S., Cosnier, S., 2016. J. Mater. Chem. A 4, 10635–10640.

Elouarzaki, K., Le Goff, A., Holzinger, M., Thery, J., Cosnier, S., 2012. J. Am. Chem. Soc. 134, 14078–14085.

Fan, Y., Liu, J.-H., Lu, H.-T., Zhang, Q., 2011. Colloids Surf. B Biointerfaces 85, 289–292.

Ghica, M.E., Carvalho, R.C., Amine, A., Brett, C.M., 2013. Sens. Actuators B Chem. 178, 270–278.

Grdeń, M., \Lukaszewski, M., Jerkiewicz, G., Czerwiński, A., 2008. Electrochimica Acta 53, 7583–7598.

Holade, Y., MacVittie, K., Conlon, T., Guz, N., Servat, K., Napporn, T.W., Kokoh, K.B., Katz, E., 2015. Electroanalysis 27, 276–280.

Holade, Y., MacVittie, K., Conlon, T., Guz, N., Servat, K., Napporn, T.W., Kokoh, K.B., Katz, E., 2014. Electroanalysis 26, 2445–2457.

Huang, T., Liu, Z., Li, Yunlong, Li, Yanqiu, Chao, L., Chen, C., Tan, Y., Xie, Q., Yao, S., Wu, Y., 2018. Anal. Chim. Acta 1013, 26–35.

Islam, M.Z., Matsuyama, N., Chen, G., Kobayashi, A., Momoi, Y., Niitsu, K., 2020. Electrochemistry 20–00044.
Jiang, T., Yan, L., Meng, Y., Xiao, M., Wu, Z., Tsiakaras, P., Song, S., 2015. Appl. Catal. B Environ. 162, 275–281.
Kim, J.H., Yoon, C.S., 2021. J. Electroanal. Chem. 115736.
Li, X., Du, X., 2017. Sens. Actuators B Chem. 239, 536–543.
Liu, H., Logan, B.E., 2004. Environ. Sci. Technol. 38, 4040–4046.
Low, C.T.J., Wills, R.G.A., Walsh, F.C., 2006. Surf. Coat. Technol. 201, 371–383.
Meng, L., Jin, J., Yang, G., Lu, T., Zhang, H., Cai, C., 2009. Anal. Chem. 81, 7271–7280.
Mergenthaler, P., Lindauer, U., Dienel, G.A., Meisel, A., 2013. Trends Neurosci. 36, 587–597.
Middaugh, J., Cheng, S., Liu, W., Wagner, R., 2006. ET J.
Pakapongpan, S., Tuantranont, A., Poo-Arporn, R.P., 2017. Sci. Rep. 7, 1–12.
Pasta, M., La Mantia, F., Cui, Y., 2010. Electrochimica Acta 55, 5561–5568.
Pourbaix, M., 1974. NACE 307.
Purkait, T., Dey, R.S., 2020. J. Electroanal. Chem. 874, 114467.
Qu, L., Dai, L., 2005. J. Am. Chem. Soc. 127, 10806–10807.
Rand, D.A.J., Woods, R., 1971. J. Electroanal. Chem. Interfacial Electrochem. 31, 29–38.
Rapoport, B.I., Kedzierski, J.T., Sarpeshkar, R., 2012. PloS One 7, e38436.
Ryu, J., Kim, H.-S., Hahn, H.T., Lashmore, D., 2010. Biosens. Bioelectron. 25, 1603–1608.
Samoson, K., Thavarungkul, P., Kanatharana, P., Limbut, W., 2019. J. Electrochem. Soc. 166, B1079.
Santiago, Ó., Navarro, E., Raso, M.A., Leo, T.J., 2016. Appl. Energy 179, 497–522.
Shu, H., Cao, L., Chang, G., He, H., Zhang, Y., He, Y., 2014. Electrochimica Acta 132, 524–532.
Su, C.-H., Sun, C.-L., Peng, S.-Y., Wu, J.-J., Huang, Y.-H., Liao, Y.-C., 2019. J. Taiwan Inst. Chem. Eng. 95, 48–54.
Sun, I.-W., Chang, J.-K., 2017. Springer, pp. 835–895.
Tian, N., Zhou, Z.-Y., Sun, S.-G., 2009. Chem. Commun. 1502–1504.
Valentini, F., Amine, A., Orlanducci, S., Terranova, M.L., Palleschi, G., 2003. Anal. Chem. 75, 5413–5421.
Vassilyev, Y.B., Khazova, O.A., Nikolaeva, N.N., 1985. J. Electroanal. Chem. Interfacial Electrochem. 196, 127–144.
Wei, L., Fan, Y.-J., Wang, H.-H., Tian, N., Zhou, Z.-Y., Sun, S.-G., 2012. Electrochimica Acta 76, 468–474.
Wilson, R., Turner, A.P.F., 1992. Biosens. Bioelectron. 7, 165–185.
Yahiro, A.T., Lee, S.M., Kimble, D.O., 1964. Biochim. Biophys. Acta BBA-Spec. Sect. Biophys. Subj. 88, 375–383.
Yan, L., Brouzgou, A., Meng, Y., Xiao, M., Tsiakaras, P., Song, S., 2014. Appl. Catal. B Environ. 150, 268–274.
Yang, L., Zhang, Y., Chu, M., Deng, W., Tan, Y., Ma, M., Su, X., Xie, Q., Yao, S., 2014. Biosens. Bioelectron. 52, 105–110.
Ye, J.-S., Chen, C.-W., Lee, C.-L., 2015. Sens. Actuators B Chem. 208, 569–574.
Zhang, J.L., Wang, Y.H., Huang, K., Huang, K.J., Jiang, H., Wang, X.M., 2021. Nano Energy 84, 105853.
Zhao, S., Tong, J., Li, Y., Sun, J., Bian, C., Xia, S., 2019. Micromachines 10, 223.

Graphical Abstract

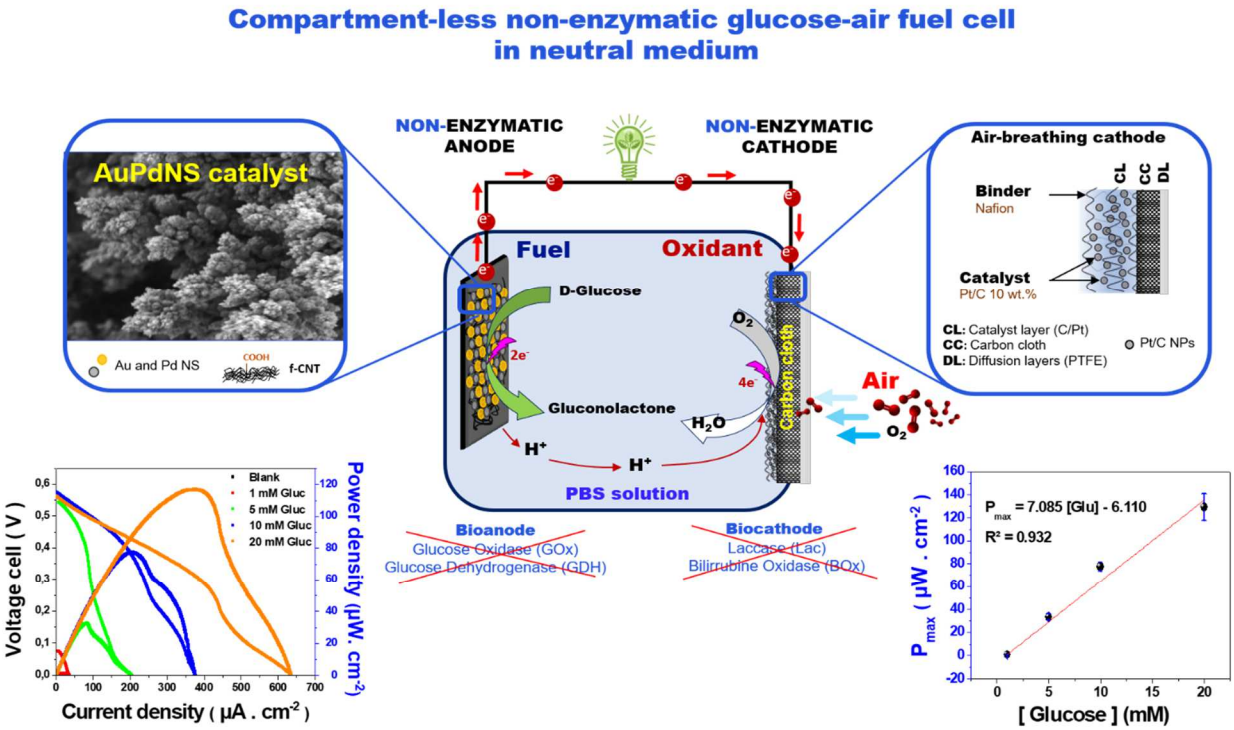

Schematic representation of the compartment-less non-enzymatic glucose/O_2 fuel cell in 0.1 M PBS (pH 7.4) based on a 3D nanostructured porous PdAu anode and an air-breathing cathode